Journal of Biomolecular NMR, 9 (1997) 94–100
ESCOM

J-Bio NMR 421

(H)N(COCA)NH and HN(COCA)NH experiments for ^{1}H-^{15}N backbone assignments in $^{13}C/^{15}N$-labeled proteins

Clay Bracken[a], Arthur G. Palmer III[a] and John Cavanagh[b,*]

[a]*Department of Biochemistry and Molecular Biophysics, Columbia University, 630 West 168th Street, New York, NY 10032, U.S.A.*
[b]*NMR Structural Biology Facility, Wadsworth Center, New York State Department of Health, P.O. Box 509, Albany, NY 12201-0509, U.S.A.*

Received 20 September 1996
Accepted 6 December 1996

Keywords: Triple resonance NMR spectroscopy; Sequential assignment; Proteins

Summary

Triple resonance HN(COCA)NH pulse sequences for correlating $^{1}H_{(i)}$, $^{15}N_{(i)}$, $^{1}H_{(i-1)}$, and $^{15}N_{(i-1)}$ spins that utilize overlapping coherence transfer periods provide increased sensitivity relative to pulse sequences that utilize sequential coherence transfer periods. Although the overlapping sequence elements reduce the overall duration of the pulse sequences, the principal benefit derives from a reduction in the number of 180° pulses. Two versions of the technique are presented: a 3D (H)N(COCA)NH experiment that correlates $^{15}N_{(i)}$, $^{1}H_{(i-1)}$, and $^{15}N_{(i-1)}$ spins, and a 3D HN(COCA)NH experiment that correlates $^{1}H_{(i)}$, $^{15}N_{(i)}$, $^{1}H_{(i-1)}$, and $^{15}N_{(i-1)}$ spins by simultaneously encoding the $^{1}H_{(i)}$ and $^{15}N_{(i)}$ chemical shifts during the t_1 evolution period. The methods are demonstrated on a $^{13}C/^{15}N$-enriched sample of the protein ubiquitin and are easily adapted for application to $^{2}H/^{13}C/^{15}N$-enriched proteins.

NMR investigations of the structures and dynamics of proteins rely on the determination of sequence-specific assignments of the backbone resonances (Cavanagh et al., 1996). Among the numerous pulse sequences developed for obtaining such assignments, the 4D HN(COCA)NH (Grzesiek et al., 1993; Hiroshi et al., 1996) utilizes the coherence transfer pathway $^{1}H_{(i)} \rightarrow {}^{15}N_{(i)} \rightarrow {}^{13}C'_{(i-1)} \rightarrow {}^{13}C^{\alpha}_{(i-1)} \rightarrow {}^{15}N_{(i-1)} \rightarrow {}^{1}H_{(i-1)}$ to generate sequential correlations between the $^{1}H_{(i)}$, $^{15}N_{(i)}$, $^{1}H_{(i-1)}$, and $^{15}N_{(i-1)}$ backbone atoms. The utility of this experiment is limited predominantly by the large $^{13}C^{\alpha}$ relaxation rates arising from dipolar coupling between the $^{13}C^{\alpha}$ and $^{1}H^{\alpha}$ spins. Complete deuteration of the protein (LeMaster et al., 1988; Grzesiek et al., 1993) reduces relaxation losses; nonetheless, as for all NMR experiments, optimization of sensitivity remains vital.

The inherent sensitivity of an NMR pulse sequence can be improved by a myriad of techniques, including reduction of the experimental duration to reduce relaxation losses (Farmer et al., 1992), utilization of more efficient coherence transfer schemes (Bax et al., 1990; Norwood et al., 1990; Palmer et al., 1991), and minimization of losses due to the number and imperfections of radiofrequency pulses (Kay et al., 1991,1993; Farmer et al., 1992; Hallenga and Lippens, 1995). In this communication we show that ^{13}CO-$^{13}C^{\alpha}$ magnetization transfer in the HN(COCA)NH experiment can be accomplished using overlapping coherence transfer steps. In this manner, the overall time and, most critically, the total number of pulses are reduced, with concomitant gain in sensitivity. Similar coherence transfer periods have been used in the HCA(CO)N (Palmer et al., 1992) and HCACO (Bazzo et al., 1995; Löhr and Rüterjans, 1995) experiments. The approach is illustrated using two 3D versions of the HN(COCA)NH experiment: the 3D (H)N(COCA)NH, which generates interresidue correlations between the $^{15}N_{(i)}$, $^{15}N_{(i-1)}$ and $^{1}H_{(i-1)}$ spins, and the 3D HN(COCA)NH, which generates interresidue correlations between $^{15}N_{(i)}$, $^{1}H_{(i)}$, $^{15}N_{(i-1)}$, and $^{1}H_{(i-1)}$ spins by using a projection technique to simultaneously frequency label the $^{1}H_{(i)}$ and the $^{15}N_{(i)}$ resonances (Szyperski et al., 1993). The sensitivities of the proposed experiments are measured as a function of temperature using $^{13}C/^{15}N$ isotopically enriched ubiquitin in order to evaluate the effect of increasing rotational correlation times.

*To whom correspondence should be addressed.

The pulse sequences for the new 3D (H)N(COCA)NH and HN(COCA)NH experiments, shown in Figs. 1a and 1b, respectively, are based on the original 4D HN-(COCA)NH experiment (Grzesiek et al., 1993), in which coherence transfer occurs sequentially via the one-bond J_{HN}, J_{NCO}, $J_{C^\alpha CO}$ and J_{NC^α} scalar coupling interactions. A 3D (H)N(COCA)NH version of the original sequence is shown in Fig. 1c. The coherence transfer schemes for the (H)N(COCA)NH experiments are discussed theoretically using the product operator formalism (Packer and Wright, 1983; Sørensen et al., 1983; Van de Ven and Hilbers, 1983). The symbols $H_{(i)\xi}$, $N_{(i)\xi}$, $C'_{(i)\xi}$, and $C^\alpha_{(i)\xi}$ (ξ = x, y, z) represent the Cartesian spin operators for the ^1H, ^{15}N, ^{13}CO, and $^{13}C^\alpha$ spins of the *i*th amino acid residue, respectively; only terms contributing to the final signal are retained.

The first INEPT sequence (Morris and Freeman, 1979) in Fig. 1a transfers ^1H magnetization to ^{15}N coherence antiphase with respect to the ^1H spin to give a density operator at point a proportional to:

$$\sigma_a = -2H_{(i)z}N_{(i)y} \qquad (1)$$

The selective H_2O 'flip-back' pulse and gradient G_1 during the INEPT sequence retain the water magnetization along the +z-axis (Grzesiek and Bax, 1993; Kay et al., 1994). During the delay 2Δ, ^{15}N coherence becomes in-phase with respect to the ^1H spin, at which point evolution of heteronucleus–proton scalar coupling interactions is halted by application of a WALTZ-16 decoupling field (Shaka and Keeler, 1987). The 90°_y pulse prior to the WALTZ-16 sequence permits the water magnetization to be spin-locked by the decoupling radiofrequency field; following decoupling, the 90°_{-y} pulse returns the water magnetization to the +z-axis (Kay et al., 1994). During the constant-time period, T, the nitrogen coherence is frequency labeled in t_1 and becomes antiphase with respect to the carbonyl spin. The simultaneous ^{15}N and ^{13}CO 90° pulses applied following T result in a density operator at point b proportional to:

$$\sigma_b = -2N_{(i)z}C'_{(i-1)y}\cos(\Omega_{Ni}t_1)\sin(\pi J_{NCO}T) \qquad (2)$$

in which Ω_{Ni} is the amide ^{15}N chemical shift for the *i*th residue.

The main improvement in the sequence presented here results from the overlapping evolution periods between points b and e. In the first period ε, evolution of the $J_{C^\alpha CO}$ one-bond scalar coupling generates ^{13}CO single-quantum coherence antiphase with respect to the $^{13}C^\alpha$ spin. The 90° $^{13}C^\alpha$ pulse converts this term into two-spin $^{13}C^\alpha$-^{13}CO multiple-quantum coherence, which is unaffected by the scalar coupling between $^{13}C^\alpha$ and ^{13}CO spins during the second period ε. During the total delay 2ε, the carbonyl coherence becomes in-phase with respect to the ^{15}N spin. At the end of the 2ε delay, a 90° ^{13}CO pulse converts the $^{13}C^\alpha$-^{13}CO multiple-quantum coherence into $^{13}C^\alpha$ single-quantum coherence that is antiphase with respect to the ^{13}CO spin. Between points d and e, the $^{13}C^\alpha$-^{13}CO scalar coupling is active for a time period ε, and the antiphase coherence becomes in-phase. Concurrently, the one-bond scalar coupling between $^{13}C^\alpha_{(i-1)}$ and $^{15}N_{(i-1)}$ and the two-bond scalar coupling between $^{13}C^\alpha_{(i-1)}$ and $^{15}N_{(i)}$ evolve for the period 2δ. The off-resonance phase shift of the ^{13}CO coherence, due to the $^{13}C^\alpha$ 90° pulse applied at c, is compensated by shifting the phase β of the ^{13}CO 90° pulse applied at d (McCoy and Mueller, 1992). The off-resonance phase shift of the $^{13}C^\alpha$ coherence, due to the ^{13}CO 90° pulse applied at d, is compensated by the ^{13}CO 90° pulse applied at e (McCoy and Mueller, 1992). The component of the density operator present at point e, which represents the desired interresidue $H_{(i)}$,$N_{(i)}$ to $H_{(i-1)}$,$N_{(i-1)}$ coherence transfer is:

$$\begin{aligned}\sigma_e = {} & 2N_{(i-1)z}C^\alpha_{(i-1)x}\cos(\Omega_{Ni}t_1)\sin(\pi J_{NCO}T) \\ & \times \sin^2(\pi J_{C^\alpha CO}\varepsilon)\sin(2\pi J_{NCO}\varepsilon)\cos(2\pi J_{C^\alpha C^\beta}\delta) \\ & \times \sin(2\pi J_{NC^\alpha}\delta)\cos(2\pi\, {}^2J_{NC^\alpha}\delta)\end{aligned} \qquad (3)$$

in which $J_{C^\alpha C^\beta}$ is the one-bond $^{13}C^\alpha$-$^{13}C^\beta$ scalar coupling constant and $^2J_{NC^\alpha}$ is the two-bond ^{15}N-$^{13}C^\alpha$ scalar coupling constant. For values of $2\delta \approx 1/J_{C^\alpha C^\beta}$, correlations in which the i–1 residue is glycine are inverted. A second term in the density operator gives rise to a weak intra-residue correlation for the *i*th residue:

$$\begin{aligned}\sigma'_e = {} & 2N_{(i)z}C^\alpha_{(i-1)x}\cos(\Omega_{Ni}t_1)\sin(\pi J_{NCO}T) \\ & \times \sin^2(\pi J_{C^\alpha CO}\varepsilon)\sin(2\pi J_{NCO}\varepsilon)\cos(2\pi J_{C^\alpha C^\beta}\delta) \\ & \times \cos(2\pi J_{NC^\alpha}\delta)\sin(2\pi\, {}^2J_{NC^\alpha}\delta)\end{aligned} \qquad (4)$$

The overlapping scheme uses the delay 2ε to refocus the ^{15}N-^{13}CO scalar coupling interaction (J_{NCO} = 15 Hz) and the delay ε to evolve the density operator under the $^{13}C^\alpha$-^{13}CO scalar coupling Hamiltonian ($J_{C^\alpha CO}$ = 55 Hz). Inevitably, the value of ε represents a compromise between optimal values for the two interactions (vide infra).

The 3D HN(COCA)NH differs from the 3D (H)N-(COCA)NH only in the initial heteronuclear transfer step, carried out using an HMQC-like coherence transfer period along with simultaneous labeling of the ^1H and ^{15}N magnetization during the constant-time evolution period (Szyperski et al., 1993). The 3D HN(COCA)NH pulse sequence is obtained by replacing the initial portion of Fig. 1a, up to the point b, with the pulse sequence elements given in Fig. 1b; the 3D HN(COCA)NH and 3D (H)N(COCA)NH sequences are identical following point b. The component of the density operator present at point e, which represents the desired interresidue $H_{(i)}$,$N_{(i)}$ to $H_{(i-1)}$,$N_{(i-1)}$ coherence transfer, is:

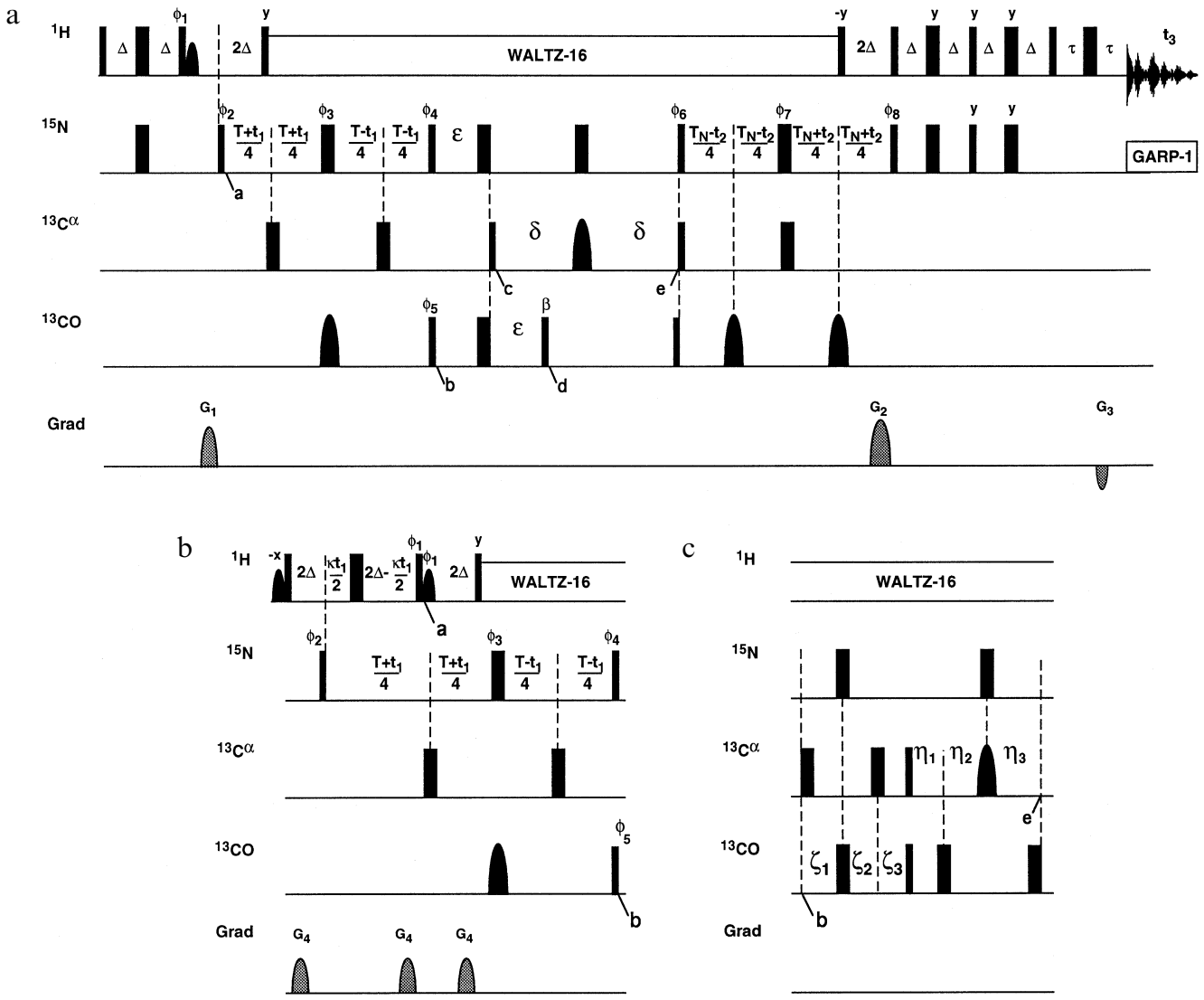

Fig. 1. Pulse sequences for the HN(COCA)NH experiments. (a) The complete pulse sequence for the 3D (H)N(COCA)NH pulse sequence, utilizing overlapping coherence transfer periods between points c and e. (b) The initial simultaneous frequency labeling period for the 3D HN(COCA)NH experiment; the complete pulse sequence is obtained by replacing elements in (a) up to the point b. (c) The original sequential ^{13}CO-$^{13}C^{\alpha}$ coherence transfer sequence; the complete pulse sequence is obtained by replacing the elements in (a) between points c and e. All spectra were recorded on a Bruker DRX-600 spectrometer equipped with a three-axis actively shielded gradient probe. The ^1H carrier was set to the H_2O frequency, the ^{15}N carrier was set to 118 ppm, the $^{13}C^{\alpha}$ carrier was set to 54 ppm, and the ^{13}CO carrier was set to 176 ppm. In the HN(COCA)NH experiment, the ^1H carrier was shifted to 6.0 ppm during the simultaneous evolution period, prior to point a. The delays Δ, T, ε, δ, T_N, and τ were set to 2.7, 22.4, 10.0, 14.2, 27.2, and 1.2 ms, respectively. The delays ζ_1, ζ_2, ζ_3, η_1, η_2, and η_3 used in the original transfer scheme were set to 11.1, 6.5, 4.6, 4.8, 9.0, and 13.8 ms, respectively (Grzesiek et al., 1993). Hard 90° and 180° pulses are denoted by thin and thick bars, respectively. Shaped pulses are indicated by rounded bars. The pulses were applied with x-phase, unless indicated otherwise. The $^{13}C^{\alpha}$ (^{13}CO) 90° and 180° pulses were set to 47.5 and 53.7 μs, respectively to provide nulls at the ^{13}CO ($^{13}C^{\alpha}$) frequency. The 180° ^{13}CO shaped pulse had a Gaussian amplitude profile truncated at the 4% level and applied at the same field strength and for twice the duration as the 180° hard ^{13}CO pulse. Shaped 180° pulses applied to $^{13}C^{\alpha}$ spins during the transfer periods involving transverse $^{13}C^{\alpha}$ magnetization had a REBURP profile (Geen and Freeman, 1991) with a peak field strength of 15.7 kHz and a duration of 400 μs. The WALTZ-16 sequence (Shaka and Keeler, 1987) with a field strength of 3.6 kHz was used to decouple the ^1H magnetization during heteronuclear coherence transfer. The GARP-1 sequence (Shaka et al., 1985) with a field strength of 1.25 kHz was used to decouple ^{15}N during acquisition. The phase cycling was as follows: $\phi_1 = 2(y),2(-y)$; $\phi_2 = x$; $\phi_3 = x,y,-x,-y$; $\phi_4 = 16(x),16(-x)$; $\phi_5 = 8(x),8(-x)$; $\beta = 334°$; $\phi_6 = x$; $\phi_7 = 4(x),4(y),4(-x),4(-y)$; $\phi_8 = x$; receiver = x,2(−x),x,−x,2(x),−x,2[−x,2(x),−x,x,2(−x),x],x,2(−x),x,−x,2(x),−x. Frequency discrimination in F1 was achieved using States–TPPI phase cycling (Marion et al., 1989b) of ϕ_2 along with the receiver phase; frequency discrimination in F2 was achieved using the PEP sensitivity-enhanced gradient method (Kay et al., 1992). The N- and P-type signals were collected separately by inverting the sign of the G_2 gradient pulse along with inversion of ϕ_8. Axial peaks were shifted to the edge of the spectrum by inverting ϕ_6 and the receiver phase for each complex t_2 point. All gradient pulses were sinusoidally shaped xyz gradient pulses. The ratios of the x, y, and z pulsed field gradients were intentionally varied between the z-filters (G_1 and G_4) and the coherence selection gradients (G_2 and G_3) to avoid accidental refocusing of residual water magnetization. The durations and maximum amplitudes were as follows: $G_1 = 2.0$ ms with $g_x = 13.8$ G/cm, $g_y = 10.2$ G/cm, $g_z = 28$ G/cm; $G_2 = 1.5$ ms with $g_x = 55.2$ G/cm, $g_y = 40.8$ G/cm, $g_z = 56$ G/cm; $G_3 = 1.5$ ms with $g_x = -5.52$ G/cm, $g_y = -4.08$ G/cm, $g_z = -5.6$ G/cm; $G_4 = 1$ ms with $g_x = 2.72$ G/cm, $g_y = 0$ G/cm and $g_z = 5.6$ G/cm.

$$\sigma_e = 2N_{(i-1)z}C^{\alpha}_{(i-1)x}\cos(\Omega_{Ni}t_1)\cos(\Omega_{Hi}\kappa t_1) \times \sin(\pi J_{NCO}T)\sin^2(\pi J_{C^{\alpha}CO}\varepsilon)\sin(2\pi J_{NCO}\varepsilon) \times \cos(2\pi J_{C^{\alpha}C^{\beta}}\delta)\sin(2\pi J_{NC^{\alpha}}\delta)\cos(2\pi\,{}^2J_{NC^{\alpha}}\delta) \quad (5)$$

Upon Fourier transformation, the F1 frequency dimension displays pairs of correlation peaks at $\Omega_{Ni} \pm \kappa\Omega_{Hi}$, in which κ is a scaling factor and Ω_{Hi} is the amide ^{1}H chemical shift for the *i*th residue. For our experiments, κ was set to 0.5, which yields a peak-to-peak separation in F1 equal to Ω_{Hi}.

The analogous version of the 3D (H)N(COCA)NH experiment utilizing the original sequential coherence transfer scheme is obtained by using the pulse elements shown in Fig. 1c to replace the overlapping coherence transfer scheme between points b and e in Fig. 1a. The component of the density operator present at point e, which represents the desired interresidue $H_{(i)}$,$N_{(i)}$ to $H_{(i-1)}$, $N_{(i-1)}$ coherence transfer, is (Grzesiek et al., 1993):

$$\sigma_e = 2N_{(i-1)z}C^{\alpha}_{(i-1)x}\cos(\Omega_{Ni}t_1)\sin(\pi J_{NCO}T) \times \sin(\pi J_{C^{\alpha}CO}\zeta_3)\sin(2\pi J_{NCO}\zeta_1)\sin(2\pi J_{C^{\alpha}CO}\eta_1) \times \cos(2\pi J_{C^{\alpha}C^{\beta}}\eta_3)\sin(2\pi J_{NC^{\alpha}N}\eta_3)\cos(2\pi\,{}^2J_{NC^{\alpha}}\eta_3) \quad (6)$$

in which $\zeta_1 = \zeta_2 + \zeta_3$ and $\eta_1 + \eta_2 = \eta_3$. Compared with the new coherence transfer sequence, the original scheme requires an additional 180° $^{13}C^{\alpha}$ pulse, applied between ζ_2 and ζ_3, and an additional 180° ^{13}CO pulse, applied between η_1 and η_2; however, independent delays $2\zeta_1$ and $2\zeta_3$ (or $2\eta_1$) are used for evolution under the ^{13}CO-^{15}N and $^{13}C^{\alpha}$-^{13}CO scalar coupling Hamiltonians, respectively.

The different pulse sequences are identical after point e. The simultaneous $^{13}C^{\alpha}$ and ^{15}N 90° pulses convert the density operator components in Eqs. 3–6 into ^{15}N coherence that is antiphase with respect to the $^{13}C^{\alpha}$ spin. A second constant-time ^{15}N evolution period is used for frequency labeling during t_2, followed by transfer back to ^{1}H for detection using a gradient version of the PEP-Z pulse sequence to maintain the water magnetization along the +z-axis (Akke et al., 1994; Muhandiram and Kay, 1994).

TABLE 1
SIGNAL-TO-NOISE RATIOS FOR 3D (H)N(COCA)NH PULSE SEQUENCES

Temperature (K)[a]	Correlation time (ns)[b]	Relative S/N[c]
300	4	1.06
285	6	1.08
277	8	1.11

[a] The temperature controller on the Bruker DRX-600 spectrometer was calibrated using a 4% CH_3OH/96% CD_3OD standard sample (Bruker Instruments, Karlsruhe, Germany).

[b] The effective correlation time was calculated using the Stokes equation.

[c] Relative S/N ratios were calculated as $[\Sigma_i(S_i^a/\sigma^a)]/[\Sigma_i(S_i^c/\sigma^c)]$, in which S_i^a and S_i^c are peak intensities and σ^a and σ^c are the standard deviations of the baseplane noise for the new (Fig. 1a) and original (Fig. 1c) versions of the 3D (H)N(COCA)NH experiment, respectively. The summations were executed for well-resolved cross peaks in the first 2D F1-F3 slices of the 3D (H)N(COCA)NH spectra. The reported results are the average of two independent trials.

The overall sensitivity of the new and original pulse sequences depends on the product of the coherence transfer functions given by the trigonometric functions in Eqs. 3–6, the damping due to relaxation of the relevant operators between points b and e, and losses from nonideal effects of the additional pulses required during the original sequence. The relative sensitivity of the pulse sequences is not affected by evolution of the density operator after point e. The relaxation damping factors, Γ, for the ^{13}CO-$^{13}C^{\alpha}$ transfer periods of Figs. 1a and 1c, respectively, are given approximately by:

$$\Gamma = \exp\{-[R(N_zC'_y) + R(C^{\alpha}_xC'_y) + R(N_zC^{\alpha}_zC'_x) + R(N_zC^{\alpha}_xC'_x)]\varepsilon/2 - [R(C^{\alpha}_x) + R(C^{\alpha}_yC'_z) + R(N_zC^{\alpha}_y) + R(N_zC^{\alpha}_xC'_z)](2\delta - \varepsilon)/4\} \quad (7)$$

$$\Gamma = \exp\{-[R(C'_x) + R(N_zC'_y) + R(C^{\alpha}_zC'_y) + R(N_zC^{\alpha}_zC'_y)]\zeta_1/2 - [R(C^{\alpha}_x) + R(C^{\alpha}_yC'_z) + R(N_zC^{\alpha}_y) + R(N_zC^{\alpha}_xC'_z)](\eta_3/2)\} \quad (8)$$

in which R(A) is the relaxation rate constant for the operator A. Because $\varepsilon \approx \zeta_1$ and $\delta \approx \eta_3$, relaxation losses for transverse operators are approximately equal for the two schemes. The shorter overlapping transfer scheme minimizes relaxation losses from ^{15}N and $^{13}C^{\alpha}$ longitudinal relaxation; however, for large proteins, these longitudinal relaxation rate constants are small. More detailed numerical calculations based on Eqs. 3 and 6–8 were performed using MATHEMATICA (Wolfram Research, Champaign, IL, U.S.A.). Relaxation rate constants were calculated for the chemical shift anisotropy mechanism, dipolar interactions between directly bonded nuclei, and dipolar interactions between heteronuclei and remote protons; cross-correlation effects were ignored. Average values of $\Sigma_j r^{-6}_{XH_j}$ equal to 0.036, 0.044, and 0.025 Å^{-6} for X = $^{13}C^{\alpha}$, ^{13}CO and ^{15}N, respectively, were used to calculate dipolar interactions with remote protons, H_j. The summation was performed over all protons not directly covalently bonded to X. The distances between nuclei, r_{XH_j} were obtained from the crystal structures of ubiquitin (Vijay-Kumar et al., 1987), calbindin D_{9k} (Svensson et al., 1992), ribonuclease H (Yang et al., 1990), tenascin fibronectin type III domain (Leahy et al., 1992), and granulocyte colony stimulating factor (Hill et al., 1993). Hydrogen atoms were built onto the heavy atoms using INSIGHT II (MSI, San Diego, CA, U.S.A.). The theoretical calcula-

tions predict a relative sensitivity of the overlapping coherence transfer scheme that ranges from 0.89 to 0.93 for rotational correlation times of 4 to 8 ns. In the absence of pulse imperfections, the overlapping transfer scheme has lower theoretical transfer efficiencies than the original sequential transfer scheme, largely because evolution times for the ^{15}N-^{13}CO scalar coupling interaction are not optimal in the overlapping scheme (vide supra). The slight improvement in sensitivity for larger rotational correlation times arises because somewhat shorter evolution periods are favored as relaxation rates increase and the misadjustment of the overlapping evolution periods becomes less severe. Thus, any empirical improvement in total sensitivity proffered by the overlapping coherence transfer scheme must be obtained principally from reduced losses due to the effect of nonideal 180° pulses (vide infra).

The new 3D (H)N(COCA)NH experiment, the new 3D HN(COCA)NH experiment, and a 3D (H)N(COCA)NH experiment using the original coherence transfer scheme were performed in duplicate on a Bruker DRX-600 NMR spectrometer. The pulses for ^{1}H, ^{15}N, $^{13}C^{\alpha}$ and ^{13}CO were generated on separate frequency synthesizer channels; the $^{13}C^{\alpha}$ and ^{13}CO low-power signals were combined and amplified by a 300 W linear amplifier (American Microwave Technologies). A 1.2 mM sample of $^{13}C/^{15}N$-labeled ubiquitin, prepared in 50 mM potassium phosphate buffer at pH 5.8, was employed for all experiments. The two 3D (H)N(COCA)NH experiments were compared at three different temperatures in order to simulate the effect of increasing molecular weight. Rotational correlation times for ubiquitin were calculated using the Stokes equation assuming $M_r = 8.5$ kDa, a radius of hydration of 3 Å, and a protein specific volume of 0.73 cm^3/g (Venable and Pastor, 1988).

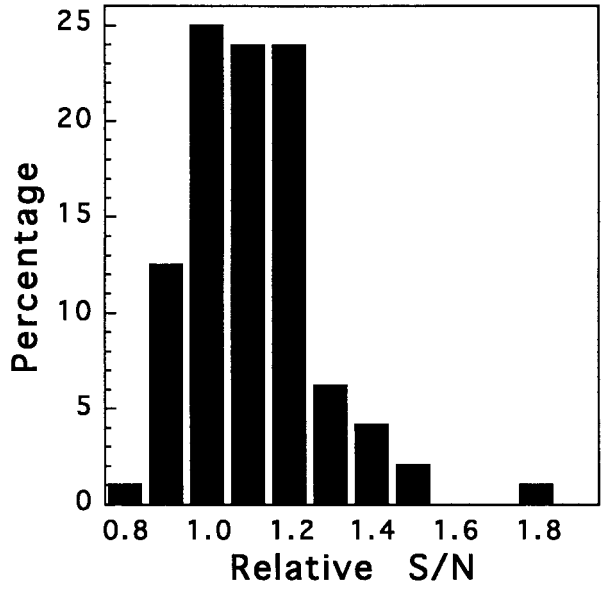

Fig. 2. Histogram displaying the relative sensitivity of the new versus the original 3D (H)N(COCA)NH experiments. Relative S/N ratios were calculated as $(S_i^a/\sigma^a)/(S_i^c/\sigma^c)$, in which S_i^a and S_i^c are the intensities of the ith peak and σ^a and σ^c are the standard deviations of the baseplane noise for the new (Fig. 1a) and original (Fig. 1c) versions of the 3D (H)N(COCA)NH experiment, respectively. A bin width of 0.1 was used in constructing the histogram. The area under the histogram has been normalized to 100%. The uncertainty in the intensity ratios was calculated to be ~0.05 by propagating the uncertainties in the peak intensities, which were assumed to be equal to $2^{1/2}$ times the standard deviation of the baseplane noise. Results are given for interresidue cross peaks in two independent pairs of experiments collected at 277 K on $^{13}C/^{15}N$-labeled ubiquitin.

The average signal-to-noise (S/N) ratios for the new 3D (H)N(COCA)NH experiment relative to the original experiment are presented as a function of temperature in Table 1, and the relative S/N ratios for individual interresidue cross peaks in 3D (H)N(COCA)NH spectra recorded at 277 K are plotted as a histogram in Fig. 2. The results in Table 1 and Fig. 2 are derived from two independent trials of the new and original versions of the experiments. The modified ^{13}CO-$^{13}C^{\alpha}$ transfer sequence shows an average increase in sensitivity of 1.08, with a slight dependence on the effective molecular correlation time. The histogram demonstrates that equal or greater sensitivity is obtained for 86% of the interresidue correlations using the new pulse sequence. As discussed above, the relative sensitivity of the two experiments is dominated by the reduction in the number of 180° pulses in the new transfer sequence, which reduces losses due to radiofrequency inhomogeneity and off-resonance effects. Comparison of the theoretical and empirical sensitivities at 300, 285 and 277 K suggests that elimination of two 180° pulses in the new experiment provides a sensitivity gain of ~1.18, which offsets the reduced theoretical coherence transfer efficiency of the overlapping coherence transfer scheme. As suggested by the theoretical sensitivity calculations (vide supra), the weak empirical dependence on the rotational correlation time may reflect differences in optimal evolution delay lengths as the relaxation rates increase; however, whether relaxation processes not incorporated into the theoretical calculations, such as cross-correlations between relaxation mechanisms, significantly affect the theoretical results is difficult to establish because both the theoretical and empirical temperature dependences are slight.

We also have observed a reduction in sensitivity if the band-selective REBURP pulses (Geen and Freeman, 1991) between the δ delays of Figs. 1a and 1b and between the η_2 and η_3 delays of Fig. 1c are replaced by rectangular 180° pulses with the radiofrequency field amplitude adjusted to yield a null in the excitation profile at the ^{13}CO resonance frequency (data not shown). The REBURP pulse efficiently inverts both $^{13}C^{\alpha}$ and $^{13}C^{\beta}$ spin operators, without perturbing the ^{13}CO spins; thus, the passive evolution of the $^{13}C^{\alpha}$-$^{13}C^{\beta}$ scalar coupling interaction is included in Eqs. 3–6. Use of a shaped pulse to

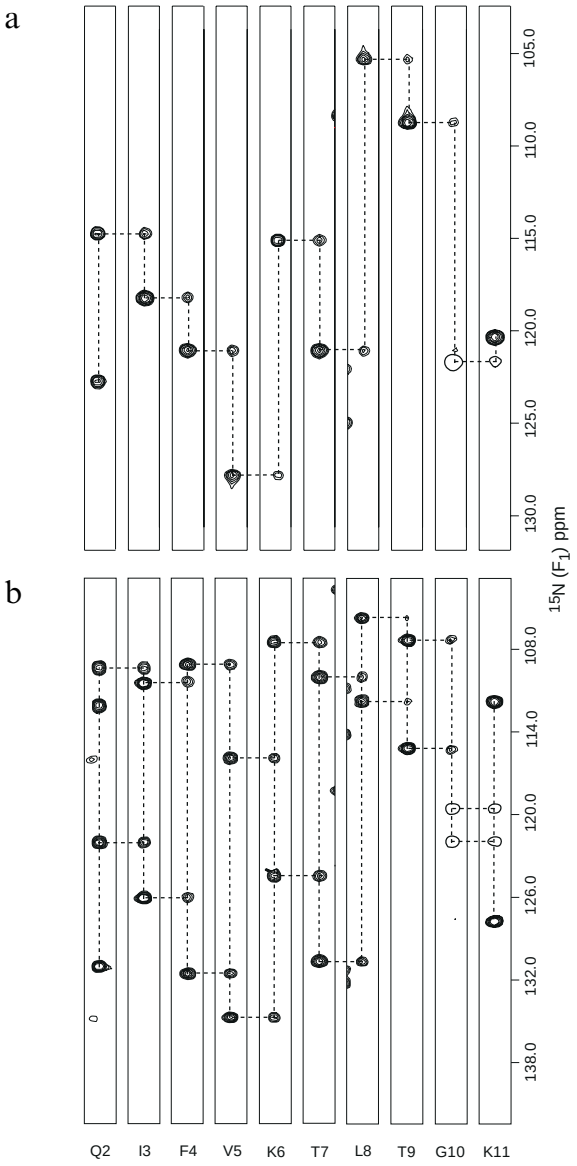

Fig. 3. Ten F1 ($^{15}N_{(i)}$) strips from the (a) 3D (H)N(COCA)NH and (b) 3D HN(COCA)NH spectra, recorded on $^{13}C/^{15}N$-labeled ubiquitin. The strips are taken at the F1 ($^{15}N_{(i-1)}$)/F3 ($^{1}H_{(i-1)}$) frequencies of residues 2 through 11 (backbone assignments for ubiquitin have been given elsewhere (Wang et al., 1995)). Correlations to Gly^{10} have negative intensities and the cross peaks are drawn with a single contour line. The (H)N(COCA)NH spectrum was acquired with 47 (t_1) × 47 (t_2) × 2048 (t_3) complex points and spectral widths of 2174 Hz (F1), 2174 Hz (F2), and 10 000 Hz (F3). The experiment was collected in 102 h using 64 scans per complex point. The HN(COCA)NH spectrum was acquired with 64 (t_1) × 32 (t_2) × 2048 (t_3) complex points with spectral widths of 3846 Hz (F1), 2174 Hz (F2), and 10 000 Hz (F3). The experiment was collected in 47 h using 32 scans per complex point. The ^{1}H splitting of the ^{15}N (F1) frequency is scaled down by a factor of $\kappa = 0.5$ and is relative to the ^{1}H carrier frequency, which was set to 6.0 ppm during the simultaneous (^{15}N-^{1}H) t_1 labeling period. The data were apodized using Kaiser functions in F1 and F2 and an exponential function in F3; the data were zero-filled once in all dimensions. The residual water signal was removed using convolution difference filtering (Marion et al., 1989a). Spectra were processed using FELIX 2.3 (MSI). Interferograms in the F1 and F2 dimensions were doubled in length by HSVD linear prediction (Barkhuijsen et al., 1987), using in-house software.

selectively invert only the $^{13}C^{\alpha}$ operators and remove the effect of the passive scalar coupling has been described (Hiroshi et al., 1996).

The temperature dependence of the S/N ratios for ubiquitin suggests that the proposed 3D (H)N(COCA)NH and 3D HN(COCA)NH experiments can be applied to protonated $^{13}C/^{15}N$-labeled proteins with molecular masses of up to ~15 kDa (~8 ns rotational correlation times) before losses from $^{13}C^{\alpha}$ relaxation become overwhelming. The PEP-Z sensitivity enhancement sequence also becomes of somewhat diminished utility for proteins with molecular masses greater than ~20 kDa (Palmer et al., 1991; Shan et al., 1996). For larger proteins, complete deuteration of the H^{α} sites is required, and deuterium decoupling must be incorporated into the pulse sequences between points c and e of Figs. 1a and 1c (Grzesiek et al., 1993).

Representative F1 ($^{15}N_{(i)}$) strip plots taken from the 3D (H)N(COCA)NH and 3D HN(COCA)NH spectra are shown in Fig. 3 to illustrate sequential assignments using these experiments. Each strip taken from the 3D (H)N(COCA)NH spectrum (Fig. 3a) displays a major interresidue i to i–1 cross peak (Eq. 3) and a minor intraresidue autocorrelation peak (Eq. 4). In the HN(COCA)NH experiment (Fig. 3b), the $^{15}N_{(i)}$ resonance signals in F1 appear as doublets separated by the $^{1}H_{(i)}$ resonance frequencies (Eq. 5). All slices show the expected cross peaks, including both intraresidue and interresidue correlations. The 3D HN(COCA)NH experiment affords greater digital resolution in the indirect dimensions than a 4D HN(COCA)NH experiment, and, compared with the 3D (H)N(COCA)NH experiment, the additional information provided by the simultaneously encoded $^{1}H_{(i)}$ resonance frequencies is useful in unambiguously determining sequential correlations. Thus, the 3D HN(COCA)NH pulse sequence provides a robust and rapid method for generating sequence-specific amide ^{1}H and ^{15}N backbone assignments. This technique should prove useful in establishing the assignments necessary for H^{N} hydrogen exchange and ^{15}N relaxation measurements in cases where complete backbone and side-chain resonance assignments are not required.

For a 3D or 4D NMR experiment with low inherent sensitivity, modest improvements can be important for a successful application of the technique because extended signal averaging is impractical. The improvement in relative sensitivity of ~1.08 obtained for the overlapping ^{13}CO-$^{13}C^{\alpha}$ coherence transfer scheme results in a ~17% reduction in the signal averaging required in the new HN(COCA)NH experiments to obtain equivalent S/N ratios as in the original experiment; in practice, time savings of 20–24 h would be obtained for experiment durations of 5–6 days. The present results reinforce the importance of 180° pulse imperfections for overall sensitivity in these and other (Farmer et al., 1992; Kay et al., 1993; Yamazaki et al., 1994; Hallenga and Lippens, 1995) NMR experiments.

Acknowledgements

We thank Lynn McNaughton for technical support. This work was supported by National Science Foundation Grant MCB9419049 (A.G.P.), an Irma T. Hirschl Career Scientist Award (A.G.P.) and a National Institutes of Health Postdoctoral Fellowship (GM17562) (C.B.).

References

Akke, M., Carr, P.A. and Palmer III, A.G. (1994) *J. Magn. Reson.*, **B104**, 298–302.

Barkhuijsen, H., De Beer, R. and Van Ormondt, D. (1987) *J. Magn. Reson.*, **73**, 553–557.

Bax, A., Ikura, M., Kay, L.E., Torchia, D.A. and Tschudin, R. (1990) *J. Magn. Reson.*, **86**, 304–318.

Bazzo, R., Cicero, D.O. and Barbato, G. (1995) *J. Magn. Reson.*, **B107**, 189–191.

Cavanagh, J., Fairbrother, W.J., Palmer III, A.G. and Skelton, N.J. (1996) *Protein NMR Spectroscopy: Principles and Practice*, Academic Press, New York, NY, U.S.A., pp. 1–587.

Farmer II, B.T., Venters, R.A., Spicer, L.D., Wittekind, M.G. and Müller, L. (1992) *J. Biomol. NMR*, **2**, 195–202.

Geen, H. and Freeman, R. (1991) *J. Magn. Reson.*, **93**, 93–141.

Grzesiek, S., Anglister, J., Ren, H. and Bax, A. (1993) *J. Am. Chem. Soc.*, **115**, 4369–4370.

Grzesiek, S. and Bax, A. (1993) *J. Am. Chem. Soc.*, **115**, 12593–12594.

Hallenga, K. and Lippens, G.M. (1995) *J. Biomol. NMR*, **5**, 59–66.

Hill, C.P., Osslund, T.D. and Eisenberg, D. (1993) *Proc. Natl. Acad. Sci. USA*, **90**, 5167–5171.

Hiroshi, M., Eriks, K. and Gerhard, W. (1996) *J. Magn. Reson.*, **B111**, 194–199.

Kay, L.E., Ikura, M. and Bax, A. (1991) *J. Magn. Reson.*, **91**, 84–92.

Kay, L.E., Keifer, P. and Saarinen, T. (1992) *J. Am. Chem. Soc.*, **114**, 10663–10665.

Kay, L.E., Xu, G.-Y., Singer, A.U., Muhandiram, D.R. and Forman-Kay, J.D. (1993) *J. Magn. Reson.*, **B101**, 333–337.

Kay, L.E., Xu, G.-Y. and Yamazaki, T. (1994) *J. Magn. Reson.*, **A109**, 129–133.

Leahy, D., Hendrickson, W.A., Aukhil, I. and Erickson, H.P. (1992) *Science*, **258**, 987–991.

LeMaster, D.M., Kay, L.E., Brünger, A.T. and Prestegard, J.H. (1988) *FEBS Lett.*, **236**, 71–76.

Löhr, F. and Rüterjans, H. (1995) *J. Magn. Reson.*, **B109**, 80–87.

Marion, D., Ikura, M. and Bax, A. (1989a) *J. Magn. Reson.*, **84**, 425–430.

Marion, D., Ikura, M., Tschudin, R. and Bax, A. (1989b) *J. Magn. Reson.*, **85**, 393–399.

McCoy, M.A. and Mueller, L. (1992) *J. Magn. Reson.*, **99**, 18–36.

Morris, G.A. and Freeman, R. (1979) *J. Am. Chem. Soc.*, **101**, 760–762.

Muhandiram, D.R. and Kay, L.E. (1994) *J. Magn. Reson.*, **B103**, 203–216.

Norwood, T.J., Boyd, J.E., Heritage, J.E., Soffe, N. and Campbell, I.D. (1990) *J. Magn. Reson.*, **87**, 488–501.

Packer, K.J. and Wright, K.M. (1983) *Mol. Phys.*, **50**, 797–813.

Palmer III, A.G., Cavanagh, J., Wright, P.E. and Rance, M. (1991) *J. Magn. Reson.*, **93**, 151–170.

Palmer III, A.G., Fairbrother, W.J., Cavanagh, J., Wright, P.E. and Rance, M. (1992) *J. Biomol. NMR*, **2**, 103–108.

Shaka, A.J., Barker, P.B. and Freeman, R. (1985) *J. Magn. Reson.*, **64**, 547–552.

Shaka, A.J. and Keeler, J. (1987) *Prog. NMR Spectrosc.*, **19**, 47–129.

Shan, X., Gardner, K.H., Muhandiram, D.R., Rao, N.S., Arrowsmith, C.H. and Kay, L.E. (1996) *J. Am. Chem. Soc.*, **118**, 6570–6579.

Sørensen, O.W., Eich, G.W., Levitt, M.H., Bodenhausen, G. and Ernst, R.R. (1983) *Prog. NMR Spectrosc.*, **16**, 163–192.

Svensson, L.A., Thulin, E. and Forsén, S. (1992) *J. Mol. Biol.*, **223**, 601–606.

Szyperski, T., Wider, G., Bushweller, J.H. and Wüthrich, K. (1993) *J. Am. Chem. Soc.*, **115**, 9307–9310.

Van de Ven, F.J.M. and Hilbers, C.W. (1983) *J. Magn. Reson.*, **54**, 512–520.

Venable, R.M. and Pastor, R.W. (1988) *Biopolymers*, **27**, 1001–1014.

Vijay-Kumar, S., Bugg, C.E. and Cook, W.J. (1987) *J. Mol. Biol.*, **194**, 531–544.

Wang, A.C., Grzesiek, S., Tschudin, R., Lodi, P.J. and Bax, A. (1995) *J. Biomol. NMR*, **5**, 376–382.

Yamazaki, T., Lee, W., Arrowsmith, C.H., Muhandiram, D.R. and Kay, L.E. (1994) *J. Am. Chem. Soc.*, **116**, 11655–11666.

Yang, W., Hendrickson, W.A., Crouch, R.J. and Satow, Y. (1990) *Science*, **249**, 1398–1405.